Active Cancellation of Periodic CM EMI at the Input of a Motor Inverter by Injecting Synthesized and Synchronized Signals (S³-AEF)

Andreas Bendicks, *Member*, andreas.bendicks@tu-dortmund.de
Michael Gerten, *Student Member*, michael.gerten@tu-dortmund.de
Stephan Frei, *Senior Member*, stephan.frei@tu-dortmund.de

***Abstract*—Active EMI cancellation is a promising solution to reduce the size of passive filters. Power electronic systems may generate periodic disturbances if they are controlled by periodic signals in steady-state operation. Periodic disturbances can be represented by a set of sine waves, according to the Fourier theory, and can be suppressed by an appropriate set of cancelling sine waves injected into the system. Since bothersome effects, like delay times or complex transfer functions, can be compensated by individually selecting the appropriate amplitude and phase for each cancelling sine wave, high EMI reductions can be achieved in a wide frequency range. In this contribution, this cancellation method is applied to the common-mode EMI of a three-phase motor inverter in stationary operation with periodic control signals in the frequency range from 150 kHz to 30 MHz. Approximately 2.4 million harmonics are suppressed. The characteristics of the overall system are discussed and the challenges for the cancellation system are elaborated. A method for the synthesis of the cancellation signal is introduced. The design of the cancellation system is described, and its signal processing is presented. The outstanding performance is proven by reference measurements in a laboratory setup. Extensions for practical applications are discussed.**

***Keywords*—Inverters; electromagnetic compatibility; electromagnetic interference; active filters; signal synthesis**

I. Introduction

Power electronic systems tend to be considerable sources of **e**lectro**m**agnetic **i**nterferences (EMI) due to the high-frequency switching of power transistors. To comply with international standards on **e**lectro**m**agnetic **c**ompatibility (EMC), e.g. CISPR 25 in automotive [1], the conducted EMI is commonly reduced by applying passive filters that are often bulky and heavy. To resolve this issue, active cancellation techniques can be applied that aim at a destructive interference between noise and anti-noise [2]. This strategy is commonly applied in acoustics and successively in EMC.

In EMC, **a**ctive **EMI** **f**ilters (AEFs) have been developed in, e.g., [3]-[6] and further analyzed and systemized in, e.g., [7] and [8]. Like passive EMI filters, AEFs are connected between the EMI source and EMI victim. These systems use analog circuitry (and rarely also digital, e.g., [9] and [10]) to generate the cancellation signal in a feedback or feedforward approach from a measured disturbance. In general, the performance of cancellation systems depends on the matching between EMI and anti-EMI [11]. For AEFs, this matching is systematically limited by finite and frequency-dependent gains of analog amplifiers (that can be interpreted as time constants) [7],[8], required stabilization elements in the closed loop of feedback AEFs [7], deviations in the signal generation of feedforward AEFs [12], delay times due to the signal propagation [11], and delay times due to the signal processing in digital variants [10],[11].

Considering (quasi-) periodic EMI, the disturbing spectrum consists of discrete and stable harmonics. So, it is feasible to synthesize a broadband cancellation signal from a set of sine waves that each cancel out the disturbing harmonic with the same frequency [11],[13]. By adjusting the amplitudes and phases of the cancelling sine waves, previously limiting effects (like time constants or delay times) can be compensated, and a very high matching between EMI and anti-EMI can be achieved. To maintain the matching and the destructive interference, the artificially synthesized cancellation signal must be synchronized to the EMI. Due to the usage of **s**ynthesized and **s**ynchronized **s**ignals (S³), it is proposed to name such a system "S³-AEF".

Until now, S³-AEF have mostly been applied to the **d**ifferential-**m**ode (DM) EMI of DC-to-DC converters in stationary operation with fixed switching frequencies (e.g. [13]-[15]). In this case, the EMI is periodic with the switching frequency, and it is sufficient to synthesize the cancellation signal from sine waves corresponding to the switching harmonics. An application of the method to motor inverters is much more complex. Due to the time-varying **p**ulse-**w**idth **m**odulation (PWM) of the inverter's half bridges, there are numerous side-band harmonics around the switching harmonics that must also be suppressed [16]. In [17], an S³-AEF has been applied to the DM EMI at the input of a motor inverter in stationary operation with periodic control signals. To suppress the EMI in the frequency range from 50 kHz to 30 MHz, the cancellation signal had to be synthesized from 2.4 million sine waves. In [18], an S³-AEF has been applied to both DC input lines of a motor inverter that is isolated from ground. A single-ended approach has been pursued in which the disturbances of the lines are individually suppressed. The disturbances on the DC input lines consist of **c**ommon-**m**ode (CM) and DM EMI. However, the performance of an S³-AEF for the suppression of CM EMI has not yet been explicitly investigated.

In this work, a new S³-AEF system is presented and discussed that suppresses the periodic CM EMI (in the frequency range from 150 kHz to 30 MHz) at the input of a motor inverter. The dimensioning of the coupling and decoupling circuits is thoroughly described. The signal processing is elaborated in detail and important extensions for prospective practical applications are discussed.

At first, the application is presented, and a generic active EMI cancellation system is introduced. The relevant system

This is the author's version of an article that has been published in the IEEE Transactions on Power Electronics.
Changes were made to this version by the publisher prior to publication.
The final version of record is available at https://doi.org/10.1109/TPEL.2022.3172205
© 2022 IEEE

characteristics are described by transfer functions that enable a convenient calculation of the required cancellation signals. For a practical realization of the S³-AEF, an algorithm is described that is based on time-domain measurements, **f**ast **F**ourier **t**ransforms (FFTs), adjustments in frequency domain and **i**nverse **f**ast **F**ourier **t**ransforms (IFFTs). The algorithm is exemplarily applied to a 48 V motor inverter system with GaN power transistors suitable for automotive applications. The inverter's control signals and the S³-AEF's cancellation signals are generated by a PC-controlled **a**rbitrary **w**aveform **g**enerator (AWG). This way, a synchronous generation of EMI and anti-EMI is ensured. The overall setup with the power electronic system and the designed S³-AEF is presented and explained. The acquired signal, the identified transfer function, and the calculated cancellation signal of the S³-AEF are discussed in detail. The active and passive EMI reductions are transparently shown by reference measurements. The results of the S³-AEF are compared to the ones of other recent active EMI filtering approaches since 2019. Last, extensions are discussed for prospective practical applications of the method. The work is closed by a conclusion.

II. Introduction of the Application and a Generic Active EMI Cancellation System

In this chapter, the application and a generic active EMI cancellation system are introduced. At first, the motor inverter in a standard EMC test setup is presented. Afterwards, the required components of a generic active EMI cancellation system are added and explained.

A. CM EMI of a Motor Inverter in a Standard Test Setup

The considered setup of the motor inverter system is depicted in Fig. 1. To drive the motor, the inverter uses three switching half bridges to generate a three-phase system from the DC supply voltage V_{supply}. The switching is the source of the EMI in the system. At the **in**put, the motor inverter has a stabilizing capacitance C_{in} that usually consists of large electrolytic and small ceramic capacitors. The motor inverter considered here is isolated from ground. In reference to the automotive standard CISPR 25 [1], the disturbances on both lines are individually measured at standardized automotive **l**ine **i**mpedance **s**tabilization **n**etworks (LISNs), called **a**rtificial **n**etworks (ANs) in the CISPR 25 automotive standard. The voltages $V_{\text{EMI,total}}^{@\text{AN,DC+}}(f)$ and $V_{\text{EMI,total}}^{@\text{AN,DC−}}(f)$ result from the CM and DM disturbances of the motor inverter according to (1) and (2) [19]:

$$V_{\text{EMI,total}}^{@\text{AN,DC+}}(f) = V_{\text{EMI,CM}}^{@\text{AN}}(f) + V_{\text{EMI,DM}}^{@\text{AN}}(f) \tag{1}$$

$$V_{\text{EMI,total}}^{@\text{AN,DC−}}(f) = V_{\text{EMI,CM}}^{@\text{AN}}(f) - V_{\text{EMI,DM}}^{@\text{AN}}(f) \tag{2}$$

The CM disturbances are mainly caused by a capacitive coupling of the half bridges' switching nodes to ground. This coupling may result from, e.g., the motor lines, the motor itself or the thermal connection of the power transistors to grounded heat sinks. For the sake of simplicity, all capacitive couplings are represented by one capacitance per line. After adding (1) and (2), the CM EMI can be determined by (3):

$$V_{\text{EMI,CM}}^{@\text{AN}}(f) = \frac{1}{2}\left[V_{\text{EMI,total}}^{@\text{AN,DC+}}(f) + V_{\text{EMI,total}}^{@\text{AN,DC−}}(f)\right] \tag{3}$$

For a practical measurement of the CM EMI, the summation of the two line disturbances $V_{\text{EMI,total}}^{@\text{AN,DC+}}(f)$ and $V_{\text{EMI,total}}^{@\text{AN,DC−}}(f)$ can be realized by using, e.g., appropriately configured high-frequency transformers [19]. Such a device is called "CM extractor" in the following. The CM extractor is terminated by the 50 Ω input of, e.g., an EMI test receiver.

B. Insertion of a Generic Active EMI Cancellation System

To suppress the CM EMI that would be emitted from the input of the motor inverter, a generic active EMI cancellation system is introduced as depicted in Fig. 2. This cancellation system is later realized as an S³-AEF. The motor inverter and the cancellation system form the **e**quipment **u**nder **t**est (EUT). To eliminate the CM EMI at the input side (that results in measurable disturbances at the ANs and the CM extractor), the AN interface port (Fig. 2) between the EUT and the AN must be free of critical CM disturbances.

The active EMI cancellation system uses a signal source that is represented as an equivalent voltage source with the voltage $V_{\text{anti,CM}}(f)$ and the internal impedance $Z_{\text{anti}}(f)$. The determination of the required cancellation signal is described in the next chapter. The cancellation source is coupled via a CM injecting circuit to the overall system. This circuit should pass the high-frequency anti-EMI and reject the possibly large operating voltages and currents of the motor inverter that could harm the cancellation source. EMI and anti-EMI (both CM) propagate through the system and superpose each other. At the AN interface port, these two signals should result in a sufficiently low residual signal due to a destructive interference. The success of the active cancellation can be evaluated by using a CM sensing circuit at the input of the EUT. Like the injecting circuit, this circuit should pass the high-frequency signals in the considered frequency range

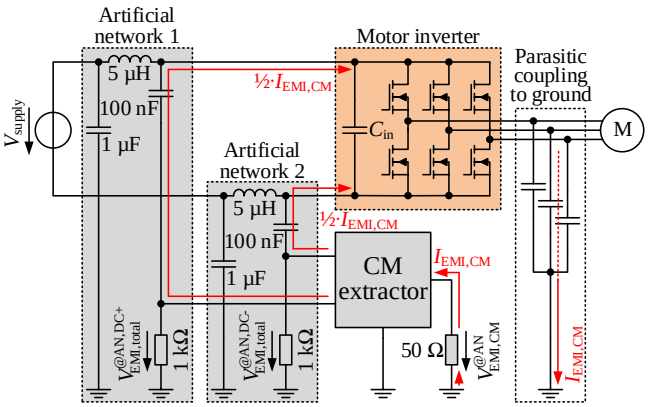

Fig. 1: Setup of the considered system.

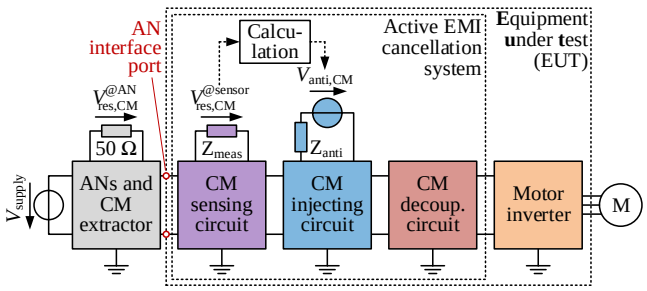

Fig. 2: Insertion of the sensing, injecting and decoupling circuits.

while rejecting the potentially harmful operating voltages and currents.

For an efficient cancellation system, the cancellation source should be strongly coupled to the AN interface port. Depending on the topology of the injecting circuit and the impedance ratios of the EMI source (motor inverter) and EMI victim (ANs and CM extractor), a large part of the cancellation signal power may flow away from the EMI victim, towards the EMI source. To avoid this problem, the injecting circuit can be decoupled from the EMI source by an appropriate decoupling circuit. As a positive side-effect, the decoupling circuit also helps in reducing the EMI by its passive attenuation.

III. Determination of the Ideal Cancellation Signal

In this chapter, the ideal cancellation signal $v_{\mathrm{anti,CM}}(t)$ is determined that can completely cancel out the EMI of the motor inverter in stationary operation with periodic control signals. To do so, the EMI and the generated anti-EMI are represented by a Fourier series each. The propagation of the anti-EMI to the sensor is described in frequency domain by using a transfer function. The superposition of EMI and anti-EMI is calculated at the sensor. From this description, the ideal complex amplitudes for the anti-EMI can conveniently be found.

A. Description of the EMI at the Sensor

The half bridges of the motor inverter generate a three-phase voltage system with the frequency f_{elec} (**elec**tric). In this work, the system is assumed to be in stationary operation (i.e. constant load and supply conditions) with periodic control signals that repeat themselves with $T_{\mathrm{elec}} = 1/f_{\mathrm{elec}}$. Due to the pole pair number p, the rotor requires the time $T_0 = pT_{\mathrm{elec}}$ to do a complete mechanical turn of 360°. As discussed in [17], the EMI of the motor inverter repeats itself with the mechanical period T_0 and mechanical frequency $f_0 = 1/T_0$. The EMI will propagate through the system and generate a voltage drop $v_{\mathrm{EMI,CM}}^{@\mathrm{sensor}}(t)$ at the sensing circuit. Due to the periodicity, it can be described by a Fourier series with complex amplitudes $V_{\mathrm{EMI,CM}}^{@\mathrm{sensor}}(kf_0)$ according to (4) [19]. The signal consists of harmonics with a spacing of f_0 [16]. This is the signal that must be cancelled out.

B. Description of the Anti-EMI at the Sensor

In analogy to (4), the generated anti-EMI $v_{\mathrm{anti,CM}}(t)$ can also be described by a Fourier series with the spacing of f_0 according to (5). This signal propagates through the overall system and superposes itself with the EMI.

To determine the effect of the anti-EMI on the sensor $v_{\mathrm{anti,CM}}^{@\mathrm{sensor}}(t)$, the propagation from the cancellation source to the sensor must be described. If the system behaves predominantly **l**inear and **t**ime-**i**nvariant (LTI) regarding the high-frequency cancellation signals, the propagation can conveniently be described in frequency domain by using a complex transfer function $H_{\mathrm{anti,CM}}^{\rightarrow\mathrm{sensor}}(f)$:

$$V_{\mathrm{anti,CM}}^{@\mathrm{sensor}}(kf_0) = H_{\mathrm{anti,CM}}^{\rightarrow\mathrm{sensor}}(kf_0) \cdot V_{\mathrm{anti,CM}}(kf_0) \tag{6}$$

C. Superposition of EMI and Anti-EMI at the Sensor

The superposition of EMI and anti-EMI at the sensor must cause a destructive interference to suppress the disturbances at the critical AN interface port. Applying the cancellation signal leads to **res**idual EMI $V_{\mathrm{res,CM}}^{@\mathrm{sensor}}(kf_0)$ according to (7):

$$V_{\mathrm{res,CM}}^{@\mathrm{sensor}}(kf_0) = V_{\mathrm{EMI,CM}}^{@\mathrm{sensor}} + \underbrace{H_{\mathrm{anti,CM}}^{\rightarrow\mathrm{sensor}} \cdot V_{\mathrm{anti,CM}}}_{=V_{\mathrm{anti,CM}}^{@\mathrm{sensor}}} \tag{7}$$

D. Calculation of the Ideal Anti-EMI

For an ideal cancellation, the residual EMI picked up by the sensor should equal 0 V:

$$\overset{(7)}{\Rightarrow} 0\ \mathrm{V} = V_{\mathrm{EMI,CM}}^{@\mathrm{sensor}} + H_{\mathrm{anti,CM}}^{\rightarrow\mathrm{sensor}} \cdot V_{\mathrm{anti,CM}} \tag{8}$$

So, the complex amplitudes $V_{\mathrm{anti,CM}}(kf_0)$ of the required cancellation signal can be found by (9):

$$\overset{(8)}{\Rightarrow} V_{\mathrm{anti,CM}}(kf_0) = -\frac{V_{\mathrm{EMI,CM}}^{@\mathrm{sensor}}(kf_0)}{H_{\mathrm{anti,CM}}^{\rightarrow\mathrm{sensor}}(kf_0)} \tag{9}$$

Even though the calculation of the required cancellation signal is – in theory – relatively simple, a realization is not trivial. The frequency spacing f_0 can be very small leading to an extremely high number of harmonics in a given frequency range. So, a very large number of complex amplitudes must be precisely identified. In the following, a method is presented to solve this problem.

IV. FFT Method for Cancellation Signal Determination and Generation

In this chapter, a method for the determination and generation of the required cancellation signal is described. Since it is fundamentally based on an FFT, it is referred to as "FFT method". First, the hardware for a digital active EMI cancellation system (S³-AEF) is presented. Afterward, the procedure of the FFT method is briefly described.

A. Digital Hardware of the S³-AEF

The digital hardware setup required for the FFT method is depicted in Fig. 3. The sensing of the disturbances can be done by using an **a**nalog-to-**d**igital **c**onverter (ADC) and a memory unit. The acquired signal is passed to a digital signal processor that runs the FFT method described in the following section. The found cancellation signal is passed to another memory unit and injected into the system by using a **d**igital-to-**a**nalog **c**onverter (DAC). Signal injection and acquisition must be done in synchronicity with the EMI and, therefore, with the motor inverter. If the motor inverter and S³-AEF are controlled by the same clock signal, the required synchronous operation can be guaranteed.

$$v_{\mathrm{EMI,CM}}^{@\mathrm{sensor}}(t) = V_{\mathrm{EMI,CM}}^{@\mathrm{sensor}}(0) + \sum_{k=1}^{\infty} 2\left|V_{\mathrm{EMI,CM}}^{@\mathrm{sensor}}(kf_0)\right| \cos\left(2\pi k f_0 t + \angle V_{\mathrm{EMI,CM}}^{@\mathrm{sensor}}(kf_0)\right) \tag{4}$$

$$v_{\mathrm{anti,CM}}(t) = V_{\mathrm{anti,CM}}(0) + \sum_{k=1}^{\infty} 2\left|V_{\mathrm{anti,CM}}(kf_0)\right| \cos\left(2\pi k f_0 t + \angle V_{\mathrm{anti,CM}}(kf_0)\right) \tag{5}$$

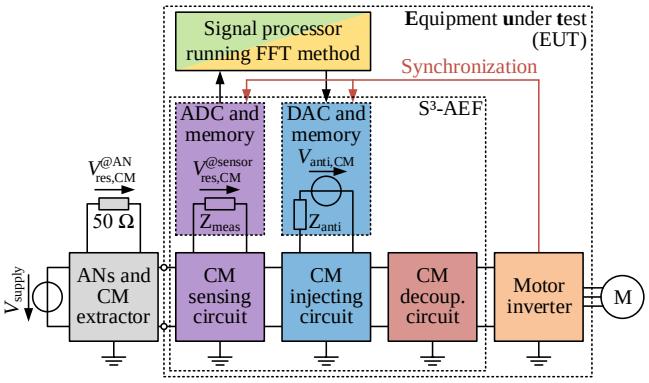

Fig. 3: Hardware setup for the overall system using the FFT method.

B. Algorithm

The fundamental goal of the algorithm is to find the required cancellation signal $v_{\mathrm{anti,CM}}(t)$ to suppress the CM EMI $v^{@\mathrm{sensor}}_{\mathrm{EMI,CM}}(t)$ at the sensor. The developed algorithm is fundamentally based on the relationship of (9) and consists of three consecutive steps that are described in the following.

In the first step, the transfer function $H^{\rightarrow\mathrm{sensor}}_{\mathrm{anti,CM}}(kf_0)$ for the anti-EM is determined by the S³-AEF. To do so, the motor inverter is deactivated. The S³-AEF injects a periodic test signal $v_{\mathrm{anti,test,CM}}(t)$ containing the frequencies of interest (synthesized from complex test amplitudes $V_{\mathrm{anti,test,CM}}(kf_0)$). At the same time, the S³-AEF acquires the system's response $v^{@\mathrm{sensor}}_{\mathrm{anti,test,CM}}(t)$ at the sensor. After acquiring at least one period of the system's response, an FFT can be done to find the complex amplitudes $V^{@\mathrm{sensor}}_{\mathrm{anti,test,CM}}(kf_0)$. Dividing these amplitudes by the test amplitudes leads to the required transfer function $H^{\rightarrow\mathrm{sensor}}_{\mathrm{anti,CM}}(kf_0)$ according to (10):

$$H^{\rightarrow\mathrm{sensor}}_{\mathrm{anti,CM}}(kf_0) = \frac{V^{@\mathrm{sensor}}_{\mathrm{anti,test,CM}}(kf_0)}{V_{\mathrm{anti,test,CM}}(kf_0)} \tag{10}$$

This transfer function respects attenuations and amplifications of the anti-EMI in its magnitude response. The phase response includes not only the phase shifts of reactive components, but also delay times of, e.g., the memory and DAC to output the anti-EMI.

In the second step, $V^{@\mathrm{sensor}}_{\mathrm{EMI,CM}}(kf_0)$ is found by deactivating the cancellation signal, activating the motor inverter, measuring the EMI at the sensor $v^{@\mathrm{sensor}}_{\mathrm{EMI,CM}}(t)$ over one or multiple periods and applying an FFT.

In the third step, $V_{\mathrm{anti,CM}}(kf_0)$ is calculated by applying (9). The corresponding time-domain signal $v_{\mathrm{anti,CM}}(t)$ is found by (5) or an IFFT.

In practical implementations, the match between EMI and anti-EMI may be limited due to, e.g., measurement noise or weak nonlinear effects. To oppose this problem, the algorithm can be iteratively applied until a given requirement is fulfilled or the hardware's limits are reached. To do so, the residual EMI $V^{@\mathrm{sensor}}_{\mathrm{res,CM}}(kf_0)$ is measured and the complex amplitudes for cancellation are corrected according to (11):

$$V_{\mathrm{anti,CM,new}}(kf_0) = V_{\mathrm{anti,CM,old}} - \underbrace{\frac{V^{@\mathrm{sensor}}_{\mathrm{res,CM}}}{H^{\rightarrow\mathrm{sensor}}_{\mathrm{anti,CM}}}}_{\text{correction}} \tag{11}$$

V. Demonstrator Setup

In this chapter, demonstrator results are presented. At first, the goal is defined. Afterward, the motor inverter and the designed S³-AEF are described. The control of the test setup and the needed signal lengths are discussed. Last, the settings for the reference measurement are stated.

A. Goal

The goal of this demonstration is to suppress the CM EMI at the DC input of a GaN motor inverter in the frequency range from 150 kHz to 30 MHz. The switching frequency is chosen to 100 kHz. The frequency f_{elec} of the three-phase system is chosen to 50 Hz. The used motor (synchronous machine) has a pole pair number p of 4. So, the harmonics will have a spacing of $f_0 = 50\ \mathrm{Hz}/4 = 12.5\ \mathrm{Hz}$. Considering the frequency range from 150 kHz to 30 MHz, there will be (30 MHz-150 kHz)/12.5 Hz + 1 ≈ 2.4 million harmonics that must be cancelled out. The fundamental period has a length of $T_0 = 1/f_0 = 1/12.5\ \mathrm{Hz} = 80\ \mathrm{ms}$.

The schematics of the complete test setup can be found in Fig. 4. A photograph of the overall test setup and the EUT can be found in Fig. 5 and Fig. 6, respectively. The setup is explained in more detail in the following.

B. Power Electronic System

The motor inverter is realized by three GaN half bridges (made of discrete transistors EPC2020 from EPC) and electrolyte capacitors with a total capacitance of approximately 25 mF to stabilize the input voltage. It is isolated from ground and has two input lines, i.e. DC+ and DC−. The supply voltage is 48 V.

The control signals for the half bridges are calculated by a PC and loaded into an **a**rbitrary **w**aveform **g**enerator (AWG) HDAWG8 from Zurich Instruments with eight channels. The HDAWG8 uses three channels to generate the three control signals (one for each half bridge). These control signals are isolated from ground by digital isolators on the control board of the inverter system (Fig. 6). During startup, the electrical frequency f_{elec} of the three-phase system is ramped up until 50 Hz is reached. Then, the control signals are periodically repeated with 50 Hz. Note that all these signals are pre-calculated by the PC and stored as arbitrary waveforms in the memory of the AWG.

The motor is operated without mechanical load. However, there are significant CM disturbances at the ANs. To avoid that ambient noise couples into the system and deteriorates the measurement results, the complete system is shielded: The inverter is built into a metal box, the motor is shielded by another metal box, and the motor lines and supply lines (between inverter and ANs) are shielded by metal coats.

C. Cancellation Source and Injecting Circuit

The HDAWG8 is not only used to generate the control signals, but also to generate the cancellation signal. The cancellation signal is calculated by a PC and stored as an arbitrary waveform in the AWG. The output of this arbitrary waveform is triggered by the control signals at the beginning of each fundamental period. This ensures a synchronous operation of the motor inverter and the anti-EMI injector. The

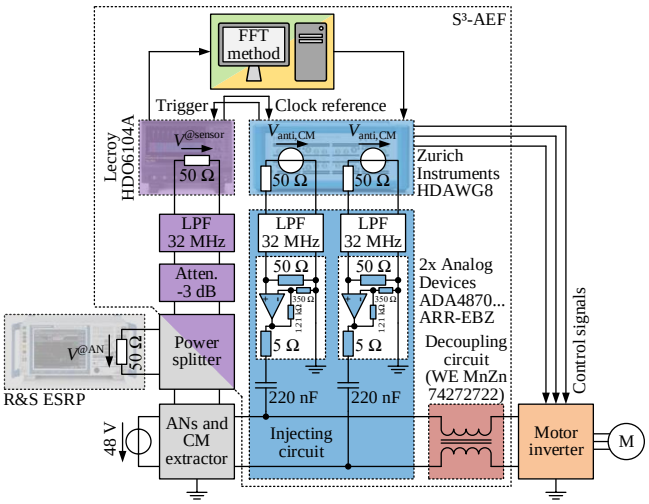

Fig. 4: Schematic of the realized test setup.

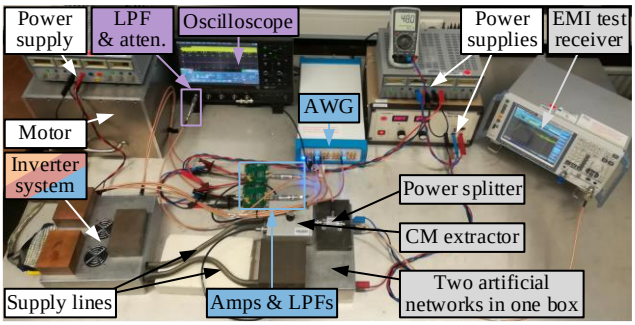

Fig. 5: Photograph of the overall test setup.

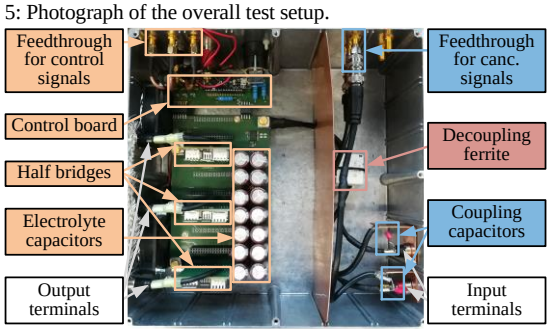

Fig. 6: Photograph of the inverter system (shielding box opened) with coupling and decoupling elements (EUT).

cancellation signal is sampled with a rate of 128 MS/s. According to the Nyquist-Shannon sampling theorem, frequencies of up to 64 MHz could be actively suppressed this way. So, it is well applicable to the considered frequency range of up to 30 MHz.

A capacitive CM injector is chosen since it is much simpler to realize than, e.g., CM transformers. As discussed already in II.B, the cancellation current may be split between the ANs and the input of the motor inverter (depending on the impedance ratios). Since the injected current shall flow to the ANs, the CM impedance of the motor inverter should be higher than the one of the ANs. Due to the large parasitic Y-capacitance of the inverter system (including the parasitic Y-capacitance of the motor), this requirement is not met. To increase the high-frequency CM input impedance of the inverter system, a decoupling CM choke is added. It is realized by applying a single split core ferrite 74272722 from **W**ürth **E**lektronik (WE) on both input lines. As a positive side-effect, the decoupling CM choke passively attenuates the disturbances. Its effect is discussed in Section VI.E.

There are two requirements for the cancellation source: First, the internal impedance should be relatively low so that the required signal can efficiently be injected. Second, the voltage range of the cancellation source must be sufficient for the required signals. The outputs of the HDAWG8 have a source impedance of 50 Ω which is too large in comparison to the impedance of the overall system. The voltage is limited to ±2.5 V which is too low. To resolve these issues a high-frequency high-power operational amplifier ADA4870 from Analog Devices is applied to each input line. These amplifier boards have an output impedance of approximately 5 Ω, and a voltage gain of 4.5. Since both channels of the AWG generate the same signal $V_{\mathrm{anti,CM}}$, a CM cancellation current is injected that depends on the CM impedances of the system. Note that it is not required to use two channels and two amplifiers. If the current-driving capabilities are large enough, one amplifier would be sufficient. However, having one channel per line can compensate system asymmetries that may introduce additional DM EMI (e.g. [18], [20] and [21]).

To avoid an increase of higher harmonics due to alias effects, **l**ow-**p**ass **f**ilters (LPFs) with a cutoff frequency of 32 MHz are applied between the AWG's channels and the amplifier boards. To ensure strong coupling of the amplifier boards, 220 nF capacitors are chosen.

D. Signal Acquisition and Sensing Circuit

Since the ANs and the CM extractor (Schwarzbeck CMDM 8700) already provide the CM EMI in this laboratory test setup, there is no need to design a CM sensing circuit for the cancellation system's signal acquisition. In practical applications, a proper CM sensing circuit is essential since there is no AN to measure at. A capacitive sensing circuit can easily be realized by two capacitors as shown in, e.g., [23]. This topic is further addressed in Chapter VIII.

The signal $V^{@\mathrm{sensor}}$ at the ANs and the CM extractor is acquired by a 12-bit resolution oscilloscope (Teledyne LeCroy HDO6104A) with a termination impedance of 50 Ω. For a precise measurement of the disturbances, only the relevant frequency range is measured by using an LPF with a cutoff frequency of 32 MHz. To avoid resonances between the overall system and the LPF, a 3 dB attenuator (50 Ω) is installed in between. The oscilloscope rescales its vertical range in every iteration to maximize the measurement precision. Oscilloscope and AWG must be synchronized for the FFT method. For this purpose, the AWG sends a trigger signal at the beginning of each fundamental period to the oscilloscope. To avoid errors due to different clock rates, the AWG uses the reference clock signal of the oscilloscope.

E. Control of the Test Setup

Both oscilloscope and AWG are controlled by a PC with MATLAB. The oscilloscope measures one complete fundamental period of the disturbances that has a length of $T_0 = 80$ ms. The PC uses the FFT method of Section IV.B to calculate the required cancellation signal (also with the length of $T_0 = 80$ ms) to suppress the ~2.4 million harmonics. Since the AWG is operated with a sampling rate of 128 MS/s, the cancellation signal consists of approximately 10.2 million samples. This signal is transferred to the AWG and injected

into the system. The corresponding signals are discussed in Section VI.

F. Reference Measurement of the CM EMI

To evaluate the performance of the S³-AEF, an ESRP EMI test receiver from Rohde & Schwarz is used. It is set up in reference to the automotive standard CISPR 25 [1] with a **r**esolution **b**and**w**idth (RBW) of 9 kHz, a measurement time of 160 ms (two fundamental periods of disturbances) and a frequency step of 2.25 kHz. To measure the spectrum in a reasonable time, an FFT-based time-domain scan is used. The disturbances are evaluated by using the average detector. A 50 Ω power splitter is applied to maintain the required termination impedance of 50 Ω for the CM extractor and to split the signal for the EMI test receiver and the oscilloscope. The power splitter attenuates the signal of the EMI test receiver by 6 dB. To compensate this effect, the spectra are mathematically increased by 6 dB after the measurement. The resulting measurement results are discussed in Section VI.E.

VI. Demonstrator Results

In this section, the results of the demonstrator setup are presented and discussed. These include the acquired disturbances at the sensor in time and frequency domain, the identified transfer function, the resulting cancellation signal in time and frequency domain, the power consumption of the S³-AEF and the final measurements at the artificial network.

A. Identified Transfer Function

At first, the S³-AEF identifies the transfer function $H_{\mathrm{anti,CM}}^{\rightarrow\mathrm{sensor}}(kf_0)$ from the cancellation sources to the sensor. To do so, the motor inverter is deactivated, and test signals are injected by the signal source of the S³-AEF. The used test signal contains harmonics between 100 kHz and 30 MHz with a spacing of 100 kHz. These harmonics have the same amplitudes and random phases. By using an IFFT, the time-domain test signal is found. It is injected into the overall system, and the system's response is measured. After applying an FFT, the transfer function can be found by applying (10). The transfer function is linearly interpolated between the measured frequencies. The result can be found in Fig. 7.

From the amplitude response, it can be found that the coupling of the cancellation source to the sensor is sufficiently strong in the complete frequency range. So, the chosen coupling and decoupling circuits prove to be appropriate. Furthermore, it can be found that the phase of the transfer function decreases almost linearly (although it cannot immediately be seen due to the logarithmic scaling of the frequency axis). Note also that the phases are limited to ±π, so the phase jumps to π if the phase drops below -π. This linear phase behavior can be traced back to a total delay time of approximately 206 ns. In this specific setup and implementation, oscilloscope and cancellation source are both triggered by the same signal. However, according to [22], it takes 180 ns for the HDAWG8 to output the signal after it is triggered. So, the generated signals are systematically delayed by 180 ns. The remaining portion of the delay time of approximately 26 ns may be explained by the time the injected cancellation signal requires to propagate through the system (i.e. cables, injectors, ANs, etc.) to the oscilloscope.

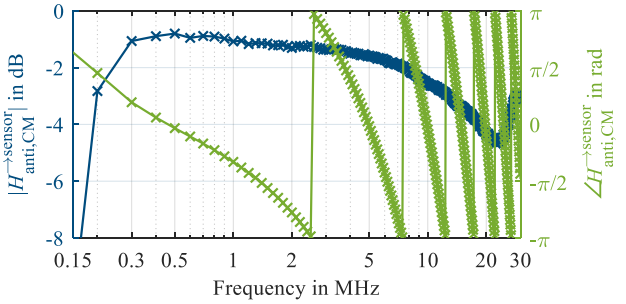

Fig. 7: Identified transfer function from cancellation source to sensor.

Note that the delay time found in $H_{\mathrm{anti,CM}}^{\rightarrow\mathrm{sensor}}(kf_0)$ only contains the propagation delay of the cancellation signals from the injector to the sensor. The time needed for signal processing (according to the FFT method of Section IV.B) has no influence here. The value of the signal processing delay is neither relevant due to the periodic and synchronous operation of the motor inverter and the S³-AEF. The S³-AEF can first acquire the disturbances, then take some time for calculations, and eventually store the found cancellation signals in the AWG. Due to the triggering of the control signals (note Section V.C), the cancellation signals will always be in sync with the disturbances, even after long signal processing times.

B. Acquired Disturbances at the Sensor

To find the disturbance spectrum, the signal source of the S³-AEF is turned off and the motor inverter is turned on. The S³-AEF acquires one total period of the disturbances that equals 80 ms as discussed before. A very short section of the disturbances at the sensor $v_{\mathrm{EMI,CM}}^{@\mathrm{sensor}}(t)$ is depicted in Fig. 8. As typical for the CM disturbances, there are high and narrow spikes that are generated due to the capacitive coupling of the switching power transistors to ground. After applying an FFT, the disturbance spectrum at the sensor $V_{\mathrm{EMI,CM}}^{@\mathrm{sensor}}(kf_0)$ is found that is depicted in Fig. 9.

C. Calculated Cancellation Signal

Since the transfer function $H_{\mathrm{anti,CM}}^{\rightarrow\mathrm{sensor}}(kf_0)$ and the disturbances $V_{\mathrm{EMI,CM}}^{@\mathrm{sensor}}(kf_0)$ are identified, the spectrum for cancellation $V_{\mathrm{anti,CM}}(kf_0)$ can be found by (9). The spectrum is depicted in Fig. 9. Since the amplitude response $|H_{\mathrm{anti,CM}}^{\rightarrow\mathrm{sensor}}(kf_0)|$ is below 0 dB, the cancellation spectrum has slightly larger harmonics than the disturbance spectrum according to (9).

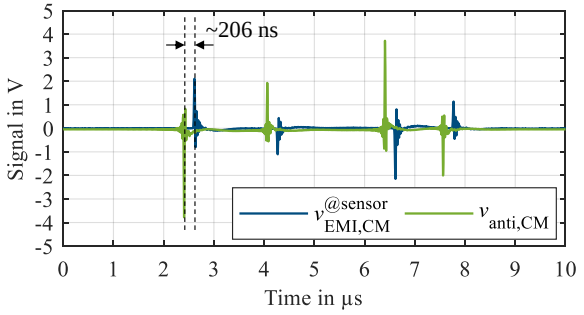

Fig. 8: Comparison of a short section of the measured disturbance signal and the calculated cancellation signal.

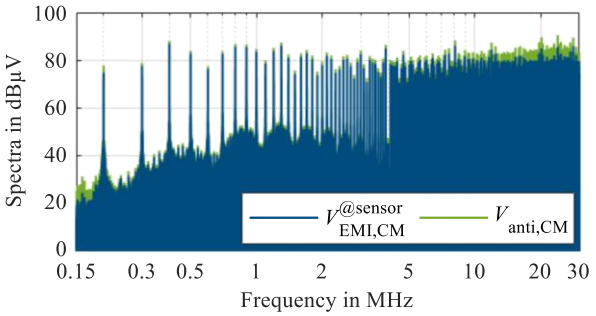

Fig. 9: Comparison of the measured disturbance spectrum and the calculated cancellation spectrum.

After applying an IFFT, the time-domain cancellation signal $v_{\text{anti,CM}}(t)$ is found. Both, the signal acquisition and the signal generation of the S³-AEF are precisely synchronized to the fundamental period of the motor inverter (note Sections V.C and V.D). This way, $v_{\text{anti,CM}}(t)$ is always synchronous to $v^{@\text{sensor}}_{\text{EMI,CM}}(t)$. A brief section of both signals is depicted in Fig. 8. Like the disturbance signal, also the cancellation signal consists of high and narrow spikes. Due to the negative sign in (9), the peaks of EMI and anti-EMI oppose each other to achieve the destructive interference. Since the cancellation spectrum is slightly larger than the disturbance spectrum, higher peaks result for the cancellation signal. As discussed in Section VI.A, the delay times of the cancellation signal are represented by phase shifts in $H^{\rightarrow\text{sensor}}_{\text{anti,CM}}(kf_0)$. By applying (9), the phases of $V_{\text{anti,CM}}(kf_0)$ are adjusted in such way that the delay times of the transfer function are compensated. These phase shifts result in a time-domain cancellation signal that is shifted by ~206 ns to earlier points in time. Injecting the anti-EMI before the actual EMI occurs is a key feature of the proposed method that allows for a high EMI reduction at high frequencies. In general, this requirement would lead to an anticausal system that requires future information for its functioning. However, due to the periodic and synchronous operation, the S³-AEF can use the information of past periods for the upcoming ones.

D. Power Consumption of the S³-AEF

The power required for S³-AEF to cancel out the EMI is only a small partition of the inverter system power. The cancellation signals $V_{\text{anti,CM}}$ injected by the operational amplifier boards ADA4870ARR-EBZ have an RMS (**r**oot **m**ean **s**quare) value of 469 mV. For a worst-case approximation of the total power of the cancellation signals, it is assumed that the termination impedance of the amplifier boards is 0 Ω and that the complete cancellation voltage drops over their internal resistance of 5 Ω. This leads to a power consumption of $2\cdot(469\text{ mV})^2/5\,\Omega \approx 88$ mW required for cancellation. Considering the DC voltage of 48 V and a DC input power of approximately 72 W, the share of the cancellation signals is only 0.12 %. This is because the CM EMI is mainly caused by parasitic couplings with rather small capacitance values. So, the CM EMI to be cancelled has a rather small power content, and only little power is required for compensation. Since the digital hardware for signal processing will introduce additional losses, an integration into available motor controllers would be advantageous (as a positive side effect, inverter and S³-AEF can easily be synchronized when they are realized on the same digital hardware). The decoupling CM choke dissipates some power of the EMI, but these losses would also occur for a CM choke in a passive filter.

E. Measurements at the Artifical Networks

The measurement results of the EMI test receiver at the ANs are depicted in Fig. 10. The first measurement shows the CM disturbances **with**o**u**t the S³-AEF (denoted by "w/o S³-AEF", note that the ANs are not removed since they belong to the test setup). The second measurement shows the CM disturbances with the installed, but deactivated S³-AEF (denoted by "with S³-AEF (off)"). The difference between these measurements represents the passive attenuation of the injecting and decoupling circuits of the S³-AEF, i.e. the passive filtering behavior. The disturbances are only slightly attenuated for the low and high ends of the considered spectrum. In between, higher attenuations are achieved. At, e.g., 2 MHz, there are CM EMI reductions of up to 30 dB.

The third measurement shows the CM disturbances with the activated S³-AEF (denoted by "with S³-AEF (on)") after the fourth iteration of the FFT method. The difference to the measurement with the deactivated S³-AEF represents the active cancellation performance of the system. The EMI is actively suppressed by very high values of approximately 65 dB at 400 kHz, 61 dB at 2 MHz and still 47 dB at 30 MHz. Similar values can also be found for the peak emissions, but these are not shown for the sake of brevity.

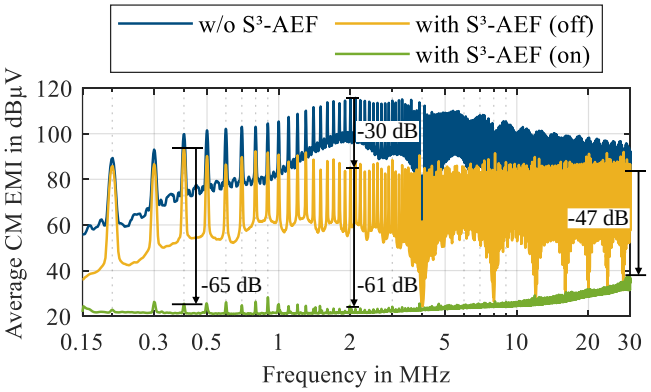

Fig. 10: Average CM disturbances measured by the EMI test receiver (spectra are increased by 6 dB to compensate the splitter's attenuation).

F. Discussion of the Active EMI Reduction

The achievable active EMI reduction is relatively constant in the complete frequency range. This has two reasons: First, the peaks of the CM disturbances (with deactivated S³-AEF) have relatively constant levels around 85 dBµV. Second, the residual disturbances (with activated S³-AEF) are suppressed down to a relatively constant noise floor of approximately 30 dBµV. The origin of this noise floor is discussed in the following.

The limiting noise floor can be traced back to the injector and sensor according to [11], [13] and [14]. Since the oscilloscope rescales itself after each iteration, it is capable of measuring very small signals. The FFT further reduces the noise floor by the so-called FFT processing gain. So, not the oscilloscope's measurement but the AWG's signal generation should be the limiting factor. The noise floor of the AWG can be transferred to the ANs by applying the

transfer function $H_{\text{anti,CM}}^{\rightarrow\text{sensor}}(kf_0)$. Since both the AWG's noise floor and the magnitude response of the transfer function are relatively constant in frequency domain, they result in a constant limit for the residual EMI.

VII. Performance Comparison with other Approaches for Active EMI Filtering

In this section, the results of the proposed S³-AEF are compared to the ones of other active EMI filtering approaches. In [24], a comprehensive summary of publications on AEFs up to the year 2019 is given. In Table I, a summary of recent publications (since 2019) on active filtering approaches can be found.

The most common approaches for active filtering apply AEFs in feedforward and/or feedback topologies ([25]-[35]). The application field comprises (motor) inverters, AC-to-DC and DC-to-DC converters. In all cases, a broadband EMI suppression can be achieved, albeit it is split into a lower and a higher frequency range in [30] and [31]. In general, it can be summarized that AEFs are most effective for frequencies from approximately 100 kHz to 1 MHz. In this frequency range, they typically achieve active EMI reductions of 20 dB to 40 dB. Noteworthy, values above 40 dB can be found in [26] and [27]. For frequencies above 1 MHz, the active EMI suppression of AEFs diminishes significantly. One exception is the extraordinary result of [31], in which a combination of a feedforward and feedback AEF leads to active EMI reductions of 15 dB at frequencies of up to 100 MHz.

TABLE I
Summary of active EMI filtering approaches reported since 2019

Ref.	Method	Active suppression	Converter	Characteristics
[25]	Feedforward AEF	26 dB at 150 kHz 16 dB at 1 MHz 10 dB at 6 MHz 0 dB at 10 MHz	Inverter	Broadband suppression
[26]	Two feedback AEFs in series	25 dB at 120 kHz 45 dB at 240 kHz 20 dB at 1 MHz 0 dB at 4 MHz	AC-to-DC	
[27]	Two-stage feedback AEF	39 dB at 170 kHz 49 dB at 400 kHz 32 dB at 1 MHz 0 dB at 3.3 MHz		
[28]	Feedback AEF	25 dB at 120 kHz 6 dB at ~1 MHz		
[29]		25 dB at 162 kHz 25 dB at 1 MHz 14 dB at 10 MHz 0 dB at 19 MHz		
[30]		15 dB at 64 kHz 0 dB at 500 kHz 7 dB at 10 MHz		Broadband suppression in a lower and a higher frequency range
[31]	Feedforward and feedback AEF	35 dB at 100 kHz 30 dB at 1 MHz 0 dB at 2.5 MHz 19 dB at 10 MHz 15 dB at 100 MHz		
[32]	Feedforward AEF	33 dB at 150 kHz 0 dB at 2.5 MHz	Motor inverter	Broadband suppression
[33]		34 dB at 150 kHz 37 dB at 1 MHz 18 dB at 10 MHz 0 dB at 20 MHz		
[34]		24 dB at 150 kHz 15 dB at 600 kHz 0 dB at 1 MHz		
[35]		24 dB at 150 kHz 17 dB at 300 kHz 19 dB at 1.5 MHz 0 dB at 3.7 MHz		
[36]	Predictive pulsed compensation	43 dB at 100 kHz 25 dB at 1 MHz 3 dB at 5 MHz	DC-to-DC	Broadband suppression, requires information on switching pulses
[14]	Parallel ANFs	53 dB at 300 kHz 48 dB at 1.8 MHz		Suppression of multiple switching harmonics
[15]	Successively applied ANF	60 dB at 300 kHz 40 dB at 30 MHz		Suppression of multiple switching harmonics, requires periodic operation
[37]	ANF	39 dB at 300 kHz	AC-to-DC	Suppression of one switching harmonic and its side-band harmonics
[38]		41 dB at 200 kHz 23 dB at 12.5 MHz	DC-to-AC	
This work	S³-AEF with FFT method	65 dB at 400 kHz 61 dB at 2 MHz 47 dB at 30 MHz	DC-to-AC	Broadband suppression, requires periodic operation

In [36], another approach is pursued in which compensation pulses are predictively injected into the system. This prediction is done with knowledge of the upcoming switching pulses of the DC-to-DC converter. The results appear to be better than the ones of most AEFs.

In [14], [15], [37] and [38], **a**daptive **n**otch **f**ilters (ANFs) are applied that are capable of suppressing narrow frequency ranges. By parallel [14] or successive [15] approaches, multiple switching harmonics can be suppressed. In [15], very high EMI reductions of 60 dB at 300 kHz and 40 dB at 30 MHz could be achieved. However, the applicability is limited since the successively applied ANF requires the disturbances to be periodic. In [37] and [38], ANFs are applied to time-varying disturbances. While the results are not as strong as the ones for DC-to-DC converters, they still surpass most of the aforementioned approaches.

In comparison to the other approaches, the S³-AEF of this work shows significantly better results in the complete frequency range from 150 kHz to 30 MHz, but its application is limited to periodic disturbances. Since the operation and disturbances of most power electronic systems are not periodic, the method should be developed further. Some ideas are addressed in the following section.

VIII. Extensions for Practical Applications

For a practical application of the proposed S³-AEF, some extensions are needed. These are discussed in the following.

First and most obvious, the S³-AEF must be realized by much simpler means than the used laboratory devices. Potential realizations may comprise powerful FPGAs or microcontrollers with appropriate ADCs, DACs and sufficiently large memory. In [15], an exemplary realization is shown for the DM EMI of a DC-to-DC converter. Specialized ASICs may be a good option as well.

Second, relatively large coupling capacitors have been used for the injecting circuit. However, they add to the total Y-capacitance that is usually restricted for safety reasons. So, for practical realizations, smaller coupling capacitances should be used. If they attenuate the cancellation signals too much, amplifiers with higher gains can be applied.

Third, a dedicated sensing circuit must be implemented since there are no ANs and CM extractors in practical applications. As mentioned above, a capacitive coupling circuit is cheap and easy to realize. Alternatively, an inductive CM current transformer can be used. The goal of the S³-AEF is to suppress the EMI emitted by the motor inverter. However, it can only minimize the EMI sensed by

its sensing circuit. Consequently, a high correlation between the sensed and the emitted EMI is needed. This can be achieved by coupling the sensing circuit as closely as possible to the lines where the EMI must be reduced (e.g. directly at the DC input terminals of the motor inverter).

Fourth, the proposed synthesis method may require a relatively long time for signal processing (FFT, IFFT, etc.). Since it must be ensured that the synthesized cancellation signal (that is based on past disturbances) still matches with the current disturbances, it is only applicable to periodic disturbances. To enable the application to changing disturbances, the method must be extended by, e.g., predictive approaches or lookup tables of cancellation signals required for different operation modes.

IX. Conclusion

In this contribution, the periodic CM EMI at the input of a motor inverter (that is driven by periodic control signals) has been actively cancelled out by injecting synthesized and synchronized cancellation signals. The disturbances consist of approximately 2.4 million harmonics in the considered frequency range (150 kHz – 30 MHz) and the cancellation signal had to be synthesized from an equal number of sine waves. An appropriate algorithm using an FFT, some calculations in frequency domain and an IFFT has been developed and analyzed. This algorithm has been applied to a prototype test setup consisting of an oscilloscope, an arbitrary waveform generator, a PC and coupling/decoupling circuits. The CM EMI measured at artificial networks (according to the automotive EMC standard CISPR 25) has been actively suppressed by 47 to 65 dB in the frequency range from 150 kHz to 30 MHz. Taking the passive attenuation of the S³-AEF's coupling capacitor and decoupling inductor into account, the CM EMI is reduced by up to 91 dB at 2 MHz. The cancellation signal's power of only 88 mW is negligible in comparison to the DC input power of 72 W. A comparison to other recent active EMI filtering approaches (since 2019) shows the high potential of the proposed S³-AEF. Extensions for prospective practical applications of this S³-AEF have been discussed.

Acknowledgment

The results of this publication go partly back to the project RobKom ("Robuste Kommunikation in autonomen Elektrofahrzeugen", grant number 16EMO0380) supported by the German Federal Ministry of Education and Research (BMBF). The responsibility for this publication is held by the authors only.

A special thanks goes to Sebastian Windhövel for providing the GaN motor inverter that he has realized during his Master's thesis.

References

[1] CISPR 25 – *Vehicles, boats and internal combustion engines – Radio disturbance characteristics – Limits and methods of measurement for the protection of on-board receivers*, 4th ed., Feb. 2015.

[2] P. Lueg, "Process of silencing sound oscillations," U.S. Patent 2 043 416, Jun. 9, 1936.

[3] S. Feng, W. Sander, and T. Wilson, "Small-capacitance nondissipative ripple filters for dc supplies," *IEEE Trans. Magn.*, vol. 6, no. 1, pp. 137-142, Mar. 1970.

[4] J. Walker, "Designing practical and effective active EMI filters," *in Proc. Powercon 11 Conf.*, Dallas, Texas, USA, 10-12 Apr. 1984, Paper I-3.

[5] L. E. LaWhite and M. F. Schlecht, "Active filters for 1-MHz power circuits with strict input/output ripple requirements," *IEEE Trans. Power Electron.*, vol. PE-2, no. 4, pp. 828-290, Oct. 1987.

[6] L. E. LaWhite and M. F. Schlecht, "Design of active ripple filters for power circuits operating in the 1-10 MHz range," *IEEE Trans. Power Electron.*, vol. 3, no. 3, pp. 310-317, Jul. 1988.

[7] N. K. Poon, J. C. P. Liu, C. K. Tse and M. H. Pong, "Techniques for input ripple current cancellation: classification and implementation [in smps]," *IEEE Trans. Power Electron.*, vol. 15, no. 6, pp. 1144-1152, Nov. 2000.

[8] Y.-C. Son and S.-K. Sul, "Generalization of active filters for EMI reduction and harmonics compensation," *IEEE Trans. Ind. Appl.*, vol. 42, no. 2, pp. 545-551, Mar./Apr. 2006.

[9] D. Hamza, M. Pahlevaninezhad and P. K. Jain, "Implementation of a novel digital active EMI technique in a DSP-based dc-dc digital controller used in electric vehicle (EV)," *IEEE Trans. Power Electron.*, vol. 28, no. 7, pp. 3126-3137, Jul. 2013.

[10] J. Ji, W. Chen, X. Yang and J. Lu, "Delay and decoupling analysis of a digital active EMI filter used in arc welding inverter," *IEEE Trans. Power Electron*, vol. 33, no. 8, pp. 6710-6722, Aug. 2018.

[11] A. Bendicks, "Active Cancellation of Electromagnetic Emissions of Power Electronic Systems by Injecting Synthesized and Synchronized Signals," Ph.D. dissertation, On-board Systems Lab, TU Dortmund University, Dortmund, Germany, 2020. [Online]. Available: https://eldorado.tu-dortmund.de/handle/2003/39212?locale=en.

[12] A. C. Chow and D. J. Perreault, "Design and evaluation of a hybrid passive/active ripple filter with voltage injection," *IEEE Trans. Aerosp. Electron. Syst.*, vol. 39, no. 2, pp. 471–480, Apr. 2003.

[13] A. Bendicks and S. Frei, "Broadband Noise Suppression of Stationary Clocked DC/DC Converters by Injecting Synthesized and Synchronized Cancellation Signals," *IEEE Trans. Power Electron.*, vol. 34, no. 11, pp. 10665-10674, Jan. 2019.

[14] A. Bendicks, T. Dörlemann, S. Frei, N. Hees, and M. Wiegand, "Active EMI Reduction of Stationary Clocked Systems by Adapted Harmonics Cancellation," *IEEE Trans. Electromagn. Compat.*, vol. 61, no. 4, pp. 998-1006, Aug. 2019.

[15] A. Bendicks, T. Osterburg, S. Frei, M. Wiegand, and N. Hees, "Wide-frequency EMI suppression of stationary clocked systems by injecting successively adapted cancellation signals," *in Proc. Int. Symp. Electromagn. Compat. Eur.*, Barcelona, Spain, 2-6 Sep. 2019, pp. 36–41.

[16] B. P. McGrath, D. G. Holmes, "A general analytical method for calculating inverter DC-link current harmonics," *IEEE Trans. Ind. Appl.*, vol. 45, no. 5, pp. 1851-1859, Sep./Oct. 2009.

[17] A. Bendicks, M. Gerten, and S. Frei, "Active Cancellation of Periodic DM EMI at the Input of a GaN Motor Inverter by Injecting Synthesized and Synchronized Signals," *in Proc. Int. Symp. Electromagn. Compat. Eur.*, Rome, Italy, 23-25 Sep. 2020.

[18] A. Bendicks, S. Windhövel, M. Gerten, S. Frei, "An Active CM and DM EMI Filter Based on Synthesized and Synchronized Signals for the DC Input of a GaN Inverter," in Proc. *PCIM Europe 2021*, Nuremberg, Germany, 3-7 May 2021, pp. 871-878.

[19] C. R. Paul, *Introduction to Electromagnetic Compatibility*, 2nd ed., Hoboken, NJ, USA: Wiley, 2006.

[20] A. Bendicks, M. Rübartsch, and S. Frei, "Simultaneous EMI suppression of the input and output terminals of a DC/DC converter by injecting multiple synthesized cancellation signals," in Proc. *Int. Symp. Electromagn. Compat. Eur.*, Barcelona, Spain, 2-6 Sep. 2019, pp. 842-847.

[21] A. Bendicks, M. Rübartsch, and S. Frei, "Active Cancellation of Periodic EMI at All Terminals of a DC-to-DC Converter by Injecting Multiple Artificially Synthesized Signals," *IEEE Electromagn. Compat. Magazine*, vol. 9, no. 3, pp. 73-80, 3rd Quarter 2020.

[22] HDAWG User Manual, Revision 21.02.0, Zurich Instruments AG, Zurich, Switzerland, 2021, p. 222.

[23] D. Shin, S. Jeong, and J. Kim, "Quantified design guidelines of a compact transformerless active EMI filter for performance, stability, and high voltage immunity," *IEEE Trans. Power. Electron.*, vol. 33, no. 8, pp. 6723–6737, Aug. 2018.

[24] B. Narayanasamy and F. Luo, “A survey of active EMI filters for conducted EMI noise reduction in power electronic converters,” *IEEE Trans. Electromagn. Compat.*, vol. 61, no. 6, pp. 2040–2049, Dec. 2019.

[25] D. Shin, S. Jeong, Y. Baek, C. Park, G. Park, and J. Kim, “A Balanced Feedforward Current-Sense Current-Compensation Active EMI Filter for Common-Mode Noise Reduction,” *IEEE Trans. Electromagn. Compat.*, vol. 62, no. 2, pp. 386-397, Apr. 2020.

[26] R. Goswami and S. Wang, “Investigation and modeling of combined feedforward and feedback control schemes to improve the performance of differential mode active EMI filters in AC-DC power converters,” *IEEE Trans. Ind. Electron.*, vol. 66, no. 8, pp. 6538–6548, Aug. 2019.

[27] K. Zhang, K.-W. Wang, and H. S.-H. Chung, “High-Attenuation Wideband Active Common-Mode EMI Filter Section,” *IEEE Trans. Power Electron.*, vol. 37, no. 5, pp. 5479-5490, May 2022.

[28] R. Goswami, S. Wang, E. Solodovnik, and K. J. Karimi, “Differential mode active EMI filter design for a boost power factor correction AC/DC converter,” *IEEE Trans. Emerg. Sel. Topics Circuits Syst.*, vol. 7, no. 1, pp. 576–590, Mar. 2019.

[29] Y. Zhou, W. Chen, X. Yang, R. Zhang, R. Yan, J. Liu, and H. Wang, “A New Integrated Active EMI Filter Topology with Both CM Noise and DM Noise Attenuation,” *IEEE Trans. Power Electron.*, vol. 37, no. 5, pp. 5466-5478, May 2022.

[30] S. Jeong, D. Shin, and J. Kim, “A transformer-isolated common-mode active EMI filter without additional components on power lines,” *IEEE Trans. Power Electron.*, vol. 34, no. 3, pp. 2244–2257, Mar. 2019.

[31] S. Takahashi, S. Ogasawara, M. Takemoto, K. Orikawa, and M. Tamate, “Common-mode voltage attenuation of an active common-mode filter in a motor drive system fed by a PWM inverter,” *IEEE Trans. Ind. Appl.*, vol. 55, no. 3, pp. 2721–2730, May/Jun. 2019.

[32] Y. Zhang, Q. Li, and D. Jiang, “A Motor CM Impedance Based Transformerless Active EMI Filter for DC-Side Common-Mode EMI Suppression in Motor Drive System,” *IEEE Trans. Power Electron.*, vol. 35, no. 10, pp. 10238-10248, Oct. 2020.

[33] S. Jeong, J. Park, and J. Kim, “A Customized Integrated Circuit for Active EMI Filter With High Reliability and Scalability,” *IEEE Trans. Power Electron.*, vol. 36, no. 11, pp. 12631-12645, Nov. 2021.

[34] Y. Zhang and D. Jiang, “An Active EMI Filter in Grounding Circuit for DC Side CM EMI Suppression in Motor Drive System,” *IEEE Trans. Power Electron.*, vol. 37, no. 3, pp. 2983-2992, Mar. 2022.

[35] B. Narayanasamy, H. Peng, Z. Yuan, A. I. Emon, and F. Luo, “Modeling and Analysis of a Differential Mode Active EMI Filter With an Analog Twin Circuit,” *IEEE Trans. Electromagn. Compat.*, vol. 62, no. 4, pp. 1591-1600, Aug. 2020.

[36] D. Müller, M. Beltle, and S. Tenbohlen, “EMI Suppression of a DC–DC Converter Using Predictive Pulsed Compensation,” *IEEE Trans. Electromagn. Compat.*, vol. 63, no. 6, pp. 2134-2142, Dec. 2021.

[37] A. Bendicks, A. Peters, and S. Frei, “FPGA-based Active Cancellation of the EMI of a Boost Power Factor Correction (PFC) by Injecting Modulated Sine Waves,” *L-EMCPA*, vol. 3, no. 1, pp. 11-14, Oct. 2020.

[38] T. Dörlemann, A. Bendicks, and S. Frei, “FPGA-based Adaptive Notch Filters for the Active Cancellation of Varying Electromagnetic Emissions of Power Electronic Inverter Systems,” *in Proc. 2021 IEEE International Joint EMC/SI/PI and EMC Europe Symposium*, Raleigh, NC, USA, 26 Jul.-13 Aug. 2021, pp. 307-312.

Andreas Bendicks (S’17-M’21) received his B.S. and M.S. degrees in electrical engineering from RWTH Aachen University, Aachen, Germany in 2013 and 2016, respectively. From September 2016 to March 2021, he has been a research assistant and doctoral student with the On-board Systems Lab, TU Dortmund University, Dortmund, Germany. There, he has worked on different methods to improve the EMC of power electronic systems. In June 2020, he received his doctoral degree on active cancellation of electromagnetic emissions of power electronic systems. From April to September 2021, he has been a developer for power modules with Infineon Technologies AG in Warstein, Germany. Since October 2021, he is a power electronics engineer with KOSTAL Industrie Elektrik GmbH in Hagen, Germany.

Michael Gerten (S’22) received the B.S. and M.S. degrees in electrical engineering and information technology from TU Dortmund University, Dortmund, Germany in 2017 and 2019, respectively. He is currently a Research Assistant with the On-board Systems Lab, TU Dortmund University, Dortmund, Germany. During and after his Master’s thesis, he dealt with active cancellation techniques for the suppression of periodic EMI of power electronic systems. Currently his main research interests are the simulation and analysis of electrical faults in automotive power supply systems.

Stephan Frei (M’97-SM’13) received his Dipl.-Ing. degree in electrical engineering from Berlin University of Technology in 1995. Between 1995 and 1999 he was a research assistant for EMC at Berlin University of Technology, Institute of Electrical Power Engineering. From there he received his Ph.D. degree in 1999. Between 1999 and 2005 he worked at the automaker AUDI AG in the development department. Here he developed and introduced new methods for the computation of EMC, antennas and signal integrity in vehicles. Furthermore he was responsible for the EMC release process of several vehicles and international standardization. In 2006 he became a professor for vehicular electronics at TU Dortmund University, where his research interests are EMC, SI, computational methods, and vehicle power supply systems. Dr. Frei is the author of more than 180 papers, and from 2008 to 2009 he served as Distinguished Lecturer for the IEEE EMC Society. From 2012 till 2020 he was Vice Dean or Dean of the Faculty for Electrical Engineering and Information Technology at TU Dortmund University.